

# On Time-Reversal Imaging by Statistical Testing

D. Ciuonzo, *Senior Member, IEEE*

**Abstract**—This letter is focused on the design and analysis of computational wideband time-reversal imaging algorithms, designed to be adaptive with respect to the noise levels pertaining to the frequencies being employed for scene probing. These algorithms are based on the concept of cell-by-cell processing and are obtained as theoretically-founded decision statistics for testing the hypothesis of single-scatterer presence (absence) at a specific location. These statistics are also validated in comparison with the maximal invariant statistic for the proposed problem.<sup>1</sup>

**Index Terms**—Composite Hypothesis Testing, Computational Time-Reversal, Invariant Detection, Imaging Functions.

## I. PROBLEM FORMULATION AND RELATED LITERATURE

**T**IME-REVERSAL (TR) techniques exploit the invariance of wave equation (in lossless and stationary media) to provide focusing on a scattering object (or radiating source). This is achieved by re-transmitting a time-reversed version of the scattered (or radiated) field collected over an array and can be achieved physically [1] or synthetically [2]. In the latter case (i.e. computational TR, C-TR) the time-reversing procedure consists in back-propagating numerically the field data by using the Green's function of the medium in which the propagation takes place.

Accordingly, C-TR provides a powerful tool to achieve scatterer detection and localization and represents the building rationale for many imaging procedures in different application contexts, such as radar imaging [3], subsurface prospecting [4], through-the-wall imaging [5] and breast cancer detection [6].

Manuscript submitted Jan. 4th, 2017; revised 28th Mar. 2017.

D. Ciuonzo is with Network Measurement and Monitoring (NM2) s.r.l., Naples, Italy (e-mail: domenico.ciuonzo@ieee.org).

<sup>1</sup>*Notation* - Lower-case (resp. Upper-case) bold letters denote column vectors (resp. matrices), with  $a_n$  (resp.  $A_{n,m}$ ) representing the  $n$ -th (resp. the  $(n,m)$ -th) element of the vector  $\mathbf{a}$  (resp. matrix  $\mathbf{A}$ );  $\mathbb{R}^N$  (resp.  $\mathbb{R}^{N \times M}$ ) and  $\mathbb{C}^N$  (resp.  $\mathbb{C}^{N \times M}$ ), are the sets of  $N$ -dimensional column vectors (resp. of  $N \times M$  dimensional matrices) of real and complex numbers;  $\mathbb{R}^+$  denotes the set of positive real-valued numbers;  $\mathcal{U}(N)$  denotes the group of  $N \times N$  unitary matrices;  $\mathbb{E}\{\cdot\}$ ,  $(\cdot)^T$ ,  $(\cdot)^\dagger$ ,  $(\cdot)^*$ ,  $\det[\cdot]$ ,  $\text{Tr}[\cdot]$ ,  $\text{vec}(\cdot)$ ,  $\|\cdot\|$  (resp.  $\|\cdot\|_F$ ),  $\Re\{\cdot\}$  and  $\Im\{\cdot\}$ , denote expectation, transpose, Hermitian, conjugate, matrix determinant and trace, matrix vectorization, Euclidean (resp. Frobenius) norm, real and imaginary part, respectively;  $\mathbf{0}_{N \times M}$  (resp.  $\mathbf{I}_N$ ) denotes the  $N \times M$  null (resp. identity) matrix;  $\mathbf{0}_N$  (resp.  $\mathbf{1}_N$ ) denotes the null (resp. ones) column vector of length  $N$ ;  $\mathbf{A} \otimes \mathbf{B}$  indicates the Kronecker product between  $\mathbf{A}$  and  $\mathbf{B}$ ;  $\text{diag}(\mathbf{v})$  denotes the diagonal matrix obtained by placing  $\mathbf{v}$  along the main diagonal;  $\mathbf{x}_{1:M}$  denotes the vector obtained by concatenation as  $\mathbf{x}_{1:M} \triangleq [\mathbf{x}_1^T \ \cdots \ \mathbf{x}_M^T]^T$ ;  $\frac{\partial f(\mathbf{x})}{\partial \mathbf{x}}$  (resp.  $\frac{\partial f(\mathbf{x})}{\partial \mathbf{x}^T}$ ) denotes the gradient of scalar-valued function  $f(\mathbf{x})$  w.r.t. vector  $\mathbf{x}$  arranged in a column (resp. a row) vector; the symbols “ $\sim$ ” and “ $\propto$ ” mean “distributed as” and “proportional to”;  $\mathbf{x} \sim \mathcal{CN}_N(\boldsymbol{\mu}, \boldsymbol{\Sigma})$  denotes a complex (proper) Gaussian-distributed vector  $\mathbf{x}$  with mean  $\boldsymbol{\mu} \in \mathbb{C}^{N \times 1}$  and covariance  $\boldsymbol{\Sigma} \in \mathbb{H}_N^{++}$ ;  $c \sim \mathcal{CX}_N^2$  (resp.  $c \sim \mathcal{CX}_N^2(\delta)$ ) denotes a Random Variable (RV) distributed according to a complex central (resp. non-central) chi-square distribution with  $M$  complex degrees of freedom (resp. with  $N$  complex degrees of freedom and noncentrality parameter  $\delta$ ), with  $c \sim \mathcal{CX}_N^2(\delta, a)$  representing a scaled non-central version;  $f \sim \mathcal{CF}_{N,M}$  (resp.  $f \sim \mathcal{CF}_{N,M}(\delta)$ ) denotes a RV distributed according to a complex central (resp. non-central) F-distribution with  $(N, M)$  complex degrees of freedom (resp. with  $(N, M)$  complex degrees of freedom and noncentrality parameter  $\delta$ );  $\mathbf{P}_a$  denotes the orthogonal projection of  $\mathbf{a}$ , i.e.  $\mathbf{P}_a \triangleq (\mathbf{a}\mathbf{a}^T)/\|\mathbf{a}\|^2$ , whereas  $\mathbf{P}_a^\perp \triangleq (\mathbf{I} - \mathbf{P}_a)$  its complement.

For this reason, theoretical limits on localization accuracy of multiple-scatterers by means of C-TR, based on the Cramér-Rao Lower Bound (CRLB), were obtained in [7] both for (linear) Born Approximated (BA) and (non-linear) Foldy-Lax (FL) scattering models.

The key entity in TR-imaging is the so-called Multistatic Data Matrix (MDM), whose entries consist of the scattered field due to each Tx-Rx pair for each probed frequency. Specifically, in this letter, we consider C-TR based localization in a multi-frequency (with  $L$  frequencies) multi-static setup. We assume that  $M$  point-like scatterers are located at unknown positions  $\{\mathbf{r}_m\}_{m=1}^M$  in  $\mathbb{R}^p$  with unknown scattering potentials  $\{\tau_{m,\ell}\}_{m=1}^M$  at  $\ell$ th angular frequency (denoted with  $\omega_\ell$ ) in  $\mathbb{C}$ . The Tx (resp. Rx) array consists of  $N_T$  (resp.  $N_R$ ) isotropic point elements (resp. receivers) located at  $\tilde{\mathbf{r}}_i \in \mathbb{R}^p$ ,  $i \in \{1, \dots, N_T\}$  (resp.  $\tilde{\mathbf{r}}_j \in \mathbb{R}^p$ ,  $j \in \{1, \dots, N_R\}$ ). The illuminators first send signals to the probed scenario (in a known homogeneous background) and the transducer array records the received signals. Thus, the model at  $\omega_\ell$  is [8]:

$$\mathbf{X}_\ell = \mathbf{A}_{R,\ell}(\mathbf{r}_{1:M}) \mathbf{M}_\ell(\mathbf{r}_{1:M}, \boldsymbol{\tau}_\ell) \mathbf{A}_{T,\ell}^T(\mathbf{r}_{1:M}) + \mathbf{W}_\ell, \quad (1)$$

where  $\mathbf{X}_\ell \in \mathbb{C}^{N_R \times N_T}$  denotes the measured MDM at  $\omega_\ell$  and  $\mathbf{W}_\ell \in \mathbb{C}^{N_R \times N_T}$  is a noise matrix such that  $\mathbf{w}_\ell \triangleq \text{vec}(\mathbf{W}_\ell) \sim \mathcal{CN}_N(\mathbf{0}_N, \sigma_\ell^2 \mathbf{I}_N)$ , where  $N \triangleq N_T N_R$ . The matrices  $\mathbf{W}_\ell$ ,  $\ell = 1, \dots, L$ , are also assumed to be mutually *uncorrelated*. Here  $\sigma_\ell^2$  is assumed known (resp. unknown) in the non-adaptive (resp. adaptive) case. Also, we have denoted: (a) the vector of scattering coefficients at  $\omega_\ell$  as  $\boldsymbol{\tau}_\ell \triangleq [\tau_{1,\ell} \ \cdots \ \tau_{M,\ell}]^T \in \mathbb{C}^M$ ; (b) the Tx (resp. Rx) array matrix at  $\omega_\ell$  as  $\mathbf{A}_{T,\ell}(\mathbf{r}_{1:M}) \in \mathbb{C}^{N_T \times M}$  (resp.  $\mathbf{A}_{R,\ell}(\mathbf{r}_{1:M}) \in \mathbb{C}^{N_R \times M}$ ), whose  $(i,j)$ th entry equals  $\mathcal{G}_\ell(\tilde{\mathbf{r}}_i, \mathbf{r}_j)$  (resp.  $\mathcal{G}_\ell(\tilde{\mathbf{r}}_i, \mathbf{r}_j)$ ), where  $\mathcal{G}_\ell(\cdot, \cdot)$  denotes the *relevant* (scalar) background *Green function* at  $\omega_\ell$  [9]. Finally, in Eq. (1) the scattering matrix is defined as  $\mathbf{M}_\ell(\mathbf{r}_{1:M}, \boldsymbol{\tau}_\ell) \triangleq \text{diag}(\boldsymbol{\tau}_\ell)$  for BA model [10], whereas for FL model [7]  $\mathbf{M}_\ell(\mathbf{r}_{1:M}, \boldsymbol{\tau}_\ell) \triangleq [\text{diag}^{-1}(\boldsymbol{\tau}_\ell) - \mathbf{S}_\ell(\mathbf{r}_{1:M})]^{-1}$  holds, where the  $(m,n)$ th entry of  $\mathbf{S}_\ell(\mathbf{r}_{1:M})$  equals  $\mathcal{G}_\ell(\mathbf{r}_m, \mathbf{r}_n)$  when  $m \neq n$  and zero otherwise.

Two popular methods for TR-imaging are the DORT [10] and the TR Multiple Signal Classification (TR-MUSIC) [8], [9], [11]. DORT method exploits the MDM spectrum so that imaging is obtained by back-propagating each single eigenvector belonging to the *signal subspace*; this allows to selectively focus on each single scatterer if they are well-resolved by the array. Differently, TR-MUSIC offers a dual viewpoint with respect to (w.r.t.) DORT, and the *orthogonal* (viz. noise) *subspace* is employed for imaging purposes. Both methods, unfortunately, *require knowledge of the number of scatterers  $M$  in the scene*, which is typically obtained via model-order selection techniques [12].

Alternatively, sub-optimal (simpler) imaging functions can

be designed based on a single scatterer model<sup>2</sup>, being capable of providing an image also in the case of *multiple scatterers* in the scene, while not requiring their exact number  $M$  (i.e. circumventing the model-order selection issue) [13]–[15]. For this reason, in what follows, we focus at design stage on a measured MDM (at  $\omega_\ell$ ) in the form  $\mathbf{X}_\ell = \mathbf{a}_{R,\ell}(\mathbf{r}_1) \tau_{1,\ell} \mathbf{a}_{T,\ell}^T(\mathbf{r}_1) + \mathbf{W}_\ell$  (i.e. the Tx and Rx array matrices collapse to column vectors) which, after  $\text{vec}(\cdot)$ , can be rewritten as:

$$\mathbf{x}_\ell = \mathbf{a}_{T,\ell}(\mathbf{r}_1) \otimes \mathbf{a}_{R,\ell}(\mathbf{r}_1) \tau_{1,\ell} + \mathbf{w}_\ell = \mathbf{b}_\ell(\mathbf{r}_1) \tau_{1,\ell} + \mathbf{w}_\ell, \quad (2)$$

where  $\mathbf{x}_\ell \triangleq \text{vec}(\mathbf{X}_\ell) \in \mathbb{C}^N$  and we have adopted the (shorthand) notation  $\mathbf{b}_\ell(\mathbf{r}_1) \triangleq \mathbf{a}_{T,\ell}(\mathbf{r}_1) \otimes \mathbf{a}_{R,\ell}(\mathbf{r}_1)$  (resp.  $\mathbf{b}_\ell$ ). Based on this model, a common approach for single ( $\ell$ th) frequency imaging is the so-called TR Matched Filter (MF) [13], formulated as:

$$I_{\text{tr}}(\mathbf{r}, \ell) = \left| \mathbf{a}_{R,\ell}^\dagger(\mathbf{r}) \mathbf{X}_\ell \mathbf{a}_{T,\ell}^*(\mathbf{r}) \right|^2; \quad (3)$$

where  $\mathbf{r}$  generically denotes the (single) scatterer *probed* location. Successively, in [15] Shi and Nehorai proposed a modification of the above imaging algorithm, based on a likelihood-maximization inspired argument:

$$I_{\text{ml}}(\mathbf{r}, \ell) = \left| \mathbf{a}_{R,\ell}^\dagger(\mathbf{r}) \mathbf{X}_\ell \mathbf{a}_{T,\ell}^*(\mathbf{r}) \right|^2 / \left( \|\mathbf{a}_{R,\ell}(\mathbf{r})\|^4 \|\mathbf{a}_{T,\ell}(\mathbf{r})\|^4 \right) \quad (4)$$

Indeed, the above imaging function can be interpreted as  $I_{\text{ml}}(\mathbf{r}, \ell) = |\hat{\tau}_\ell(\mathbf{r})|^2$ , where  $\hat{\tau}_\ell(\mathbf{r})$  is the Maximum Likelihood (ML) estimate of  $\tau_\ell$  (assuming  $\mathbf{r}$  *known*) for the model in (2). Similarly, in [14] a multi-frequency (wideband) imaging algorithm, based on true concentrated (w.r.t.  $\tau_\ell$ 's) likelihood-maximization (termed “likelihood imaging”) was proposed:

$$I_{\text{li}}(\mathbf{r}) = \prod_{\ell=1}^L 1 / \left\| \mathbf{P}_{\mathbf{b}_\ell(\mathbf{r})}^\perp \mathbf{x}_\ell \right\|^2. \quad (5)$$

In this letter, we start from the same rationale as the aforementioned works, by considering a single-source model. However, we depart from the aforementioned approaches by constructing imaging functions based on decision statistics which test the presence of a single scatterer located at  $\mathbf{r}$ . Precisely, the aforementioned statistics originate from theoretically-founded approaches for the following (composite) hypothesis testing:

$$\begin{cases} \mathcal{H}_0 : & \mathbf{x}_\ell = \mathbf{w}_\ell, & \ell = 1, \dots, L \\ \mathcal{H}_1 : & \mathbf{x}_\ell = \mathbf{b}_\ell(\mathbf{r}) \tau_\ell + \mathbf{w}_\ell, & \ell = 1, \dots, L \end{cases} \quad (6)$$

By denoting a generic statistic with  $t(\mathbf{x}_{1:L}, \mathbf{r})$ , the corresponding image is then formed by *varying*  $\mathbf{r}$ . It is worth remarking that the proposed approach is widely used in radar-related applications, and it naturally arises from a cell-by-cell processing rationale [16]. One of the main contributions of this letter is the design of imaging functions based on the well-known Generalized Likelihood Ratio (GLR), Rao and Wald statistics [17] for the C-TR imaging problem. The scope of the present study also includes their statistical characterization. Both adaptive ( $\tau_\ell$  is unknown,  $\sigma_\ell^2$  is a nuisance parameter) and non-adaptive ( $\tau_\ell$  is unknown,  $\sigma_\ell^2$  is known) cases will be

<sup>2</sup>It is worth noticing that the single-target model is coincident for both BA and FL models, as there is no mutual interaction effects among scatterers.

analyzed (as opposed to [13]–[15]), in order to draw interesting comparisons with the imaging functions reported in Eqs. (3), (4) and (5), respectively. In the adaptive case, also the Constant False-Alarm Rate (CFAR) behaviour of the building decision statistics is thoroughly investigated, by means of statistical invariance tools [18].

The rest of paper is organized as follows: Sec. II tackles the imaging task as a composite hypothesis test and theoretically-founded decision statistics are proposed; Sec. III analyzes their CFAR behaviour via invariance theory, while in Sec. IV a theoretical performance analysis of the corresponding imaging functions is provided. Furthermore, Sec. V provides a simulation-based analysis of GLR-, Rao- and Wald-originated imaging functions. Finally, conclusions are in Sec. VI.

## II. NON-ADAPTIVE VS. ADAPTIVE DECISION STATISTICS

In this section we develop decision statistics based on theoretically-founded criteria which will be used as the basis for the development of corresponding imaging functions, focusing on the specific instances of the GLR, Rao and Wald statistics [17] for the problem investigated. With this intent, we define, for notation compactness:  $\boldsymbol{\theta}_{r,\ell} \triangleq [\Re\{\tau_\ell\} \ \Im\{\tau_\ell\}]^T$  (unknown signal parameters at  $\omega_\ell$ );  $\boldsymbol{\theta}_{s,\ell} \triangleq \sigma_\ell^2$  (nuisance parameter at  $\omega_\ell$ );  $\boldsymbol{\theta}_\ell \triangleq [\boldsymbol{\theta}_{r,\ell}^T \ \boldsymbol{\theta}_{s,\ell}^T]^T$  (unknown parameters set at  $\omega_\ell$ );  $\boldsymbol{\theta}_r \triangleq [\boldsymbol{\theta}_{r,1}^T \ \dots \ \boldsymbol{\theta}_{r,L}^T]^T$  (overall set of unknown signal parameters);  $\boldsymbol{\theta}_s \triangleq [\boldsymbol{\theta}_{s,1}^T \ \dots \ \boldsymbol{\theta}_{s,L}^T]^T$  (overall set of nuisance parameters);  $\boldsymbol{\theta} \triangleq [\boldsymbol{\theta}_r^T \ \boldsymbol{\theta}_s^T]^T$  (overall set of unknown parameters). Based on these definitions, in the non-adaptive case  $\boldsymbol{\theta}_s = \boldsymbol{\theta}_{s,\ell} = \{\emptyset\}$  and  $\boldsymbol{\theta} = \boldsymbol{\theta}_r$  hold, respectively.

Additionally, the pdf of the  $L$  MDMs is expanded as  $f_1(\mathbf{x}_{1:L}; \boldsymbol{\theta}_r, \boldsymbol{\theta}_s) = \prod_{\ell=1}^L f_1(\mathbf{x}_\ell; \boldsymbol{\theta}_\ell)$  (due to independence of noise matrices  $\mathbf{W}_\ell$  among frequencies), where:

$$f_1(\mathbf{x}_\ell; \boldsymbol{\theta}_\ell) = (\pi \sigma_\ell^2)^{-N} \exp\left(-\|\mathbf{x}_\ell - \mathbf{b}_\ell \tau_\ell\|^2 / \sigma_\ell^2\right), \quad (7)$$

whereas the corresponding pdf under  $\mathcal{H}_0$  is  $f_0(\mathbf{x}_{1:L}; \boldsymbol{\theta}_s) = \prod_{\ell=1}^L f_0(\mathbf{x}_\ell; \boldsymbol{\theta}_{s,\ell})$ , where  $f_0(\mathbf{x}_\ell; \boldsymbol{\theta}_{s,\ell})$  is obtained by setting  $\tau_\ell = 0$  in (7). We remark that the composite hypothesis testing tackled in what follows is based on assumption of a *known* target position  $\mathbf{r}$ . Consequently,  $\mathbf{a}_{T,\ell}$  and  $\mathbf{a}_{R,\ell}$  (and so  $\mathbf{b}_\ell$ ) are assumed to be *known*. Also, given the MDMs independence among frequencies, the GLR, Rao and Wald statistics assume the simplified expressions [17]:

$$\begin{aligned} & \prod_{\ell=1}^L f_1(\mathbf{x}_\ell; \hat{\boldsymbol{\theta}}_{1,\ell}) / f_0(\mathbf{x}_\ell; \hat{\boldsymbol{\theta}}_{0,s,\ell}) \\ & \sum_{\ell=1}^L \left. \frac{\partial \ln f_1(\mathbf{x}_\ell; \boldsymbol{\theta}_\ell)}{\partial \boldsymbol{\theta}_{r,\ell}^T} \right|_{\boldsymbol{\theta}_\ell = \hat{\boldsymbol{\theta}}_{0,\ell}} [\mathbf{I}_\ell^{-1}(\hat{\boldsymbol{\theta}}_{0,\ell})]_{\boldsymbol{\theta}_{r,\ell}, \boldsymbol{\theta}_{r,\ell}} \left. \frac{\partial \ln f_1(\mathbf{x}_\ell; \boldsymbol{\theta}_\ell)}{\partial \boldsymbol{\theta}_{r,\ell}} \right|_{\boldsymbol{\theta}_\ell = \hat{\boldsymbol{\theta}}_{0,\ell}} \\ & \sum_{\ell=1}^L (\hat{\boldsymbol{\theta}}_{1,r,\ell} - \boldsymbol{\theta}_{0,r,\ell})^T \{ [\mathbf{I}_\ell^{-1}(\hat{\boldsymbol{\theta}}_{1,\ell})]_{\boldsymbol{\theta}_{r,\ell}, \boldsymbol{\theta}_{r,\ell}} \}^{-1} (\hat{\boldsymbol{\theta}}_{1,r,\ell} - \boldsymbol{\theta}_{0,r,\ell}). \end{aligned} \quad (8)$$

where  $\mathbf{I}_\ell(\boldsymbol{\theta}) \triangleq \mathbb{E} \left\{ \frac{\partial \ln f_1(\mathbf{x}_\ell; \boldsymbol{\theta}_\ell)}{\partial \boldsymbol{\theta}_\ell} \frac{\partial \ln f_1(\mathbf{x}_\ell; \boldsymbol{\theta}_\ell)}{\partial \boldsymbol{\theta}_\ell^T} \right\}$  denotes the contribution of Fisher information matrix pertaining to  $\omega_\ell$  and  $[\mathbf{I}_\ell^{-1}(\boldsymbol{\theta})]_{\boldsymbol{\theta}_{r,\ell}, \boldsymbol{\theta}_{r,\ell}}$  indicates the sub-matrix obtained by selecting from its inverse only the elements corresponding to  $\boldsymbol{\theta}_{r,\ell}$ .

Additionally, we have defined  $\widehat{\boldsymbol{\theta}}_{0,\ell} \triangleq \begin{bmatrix} \boldsymbol{\theta}_{0,r,\ell}^T & \widehat{\boldsymbol{\theta}}_{0,s,\ell}^T \end{bmatrix}^T$  (resp.  $\widehat{\boldsymbol{\theta}}_{1,\ell} \triangleq \begin{bmatrix} \widehat{\boldsymbol{\theta}}_{1,r,\ell}^T & \widehat{\boldsymbol{\theta}}_{1,s,\ell}^T \end{bmatrix}^T$ ), with  $\boldsymbol{\theta}_{0,r,\ell} \triangleq \mathbf{0}_2$  (resp. with  $\widehat{\boldsymbol{\theta}}_{1,r,\ell}$  denoting the ML estimate of  $\boldsymbol{\theta}_{r,\ell}$  under  $\mathcal{H}_1$ ) and  $\widehat{\boldsymbol{\theta}}_{0,s,\ell}$  (resp.  $\widehat{\boldsymbol{\theta}}_{1,s,\ell}$ ) denoting the ML estimate of  $\boldsymbol{\theta}_{s,\ell}$  under  $\mathcal{H}_0$  (resp. under  $\mathcal{H}_1$ ).

Based on this simplification and exploiting the key result provided in the literature (e.g. [17]) regarding the closed form of the  $\ell$ th term of each statistic in (8), we obtain the final statistic<sup>3</sup>  $t_{\text{na}} = \sum_{\ell=1}^L (\mathbf{x}_\ell^\dagger \mathbf{P}_{\mathbf{b}_\ell} \mathbf{x}_\ell) / \sigma_\ell^2$  in the *non-adaptive* case, while in the *adaptive* case it can be shown that<sup>4</sup>:

$$t_{\text{glr}} = \prod_{\ell=1}^L (1 + \Xi_\ell), \quad t_{\text{rao}} = \sum_{\ell=1}^L \frac{\Xi_\ell}{\Xi_\ell + 1}, \quad t_{\text{wald}} = \sum_{\ell=1}^L \Xi_\ell, \quad (9)$$

where we have exploited the definitions

$$\Xi_\ell \triangleq (\mathbf{x}_\ell^\dagger \mathbf{P}_{\mathbf{b}_\ell} \mathbf{x}_\ell) / (\mathbf{x}_\ell^\dagger \mathbf{P}_{\mathbf{b}_\ell}^\perp \mathbf{x}_\ell), \quad \ell = 1, \dots, L. \quad (10)$$

The proposed imaging functions are then obtained by varying  $\mathbf{r}$ . Some remarks are now in order. First, it is apparent that in the non-adaptive case the imaging function  $t_{\text{na}}(\mathbf{r})$  is a weighted sum (via  $1/\sigma_\ell^2$ ) of  $L$  terms, each corresponding to a single frequency. Interestingly, for  $L = 1$ ,  $t_{\text{na}}(\mathbf{r})$  assumes an expression which is comparable with the imaging functions in (3) and (4). Indeed, for the generic  $\omega_\ell$ ,  $t_{\text{na}}(\mathbf{r})$  simplifies to:

$$t_{\text{na}}(\mathbf{r}) = \frac{(\mathbf{x}_\ell^\dagger \mathbf{P}_{\mathbf{b}_\ell(\mathbf{r})} \mathbf{x}_\ell)}{\sigma_\ell^2} \propto \left\| \mathbf{P}_{\mathbf{a}_{R,\ell}(\mathbf{r})} \mathbf{X}_\ell \mathbf{P}_{\mathbf{a}_{T,\ell}(\mathbf{r})}^T \right\|_F^2 \quad (11)$$

$$= \left| \mathbf{a}_{R,\ell}^\dagger(\mathbf{r}) \mathbf{X}_\ell \mathbf{a}_{T,\ell}^*(\mathbf{r}) \right|^2 / \left\{ \|\mathbf{a}_{R,\ell}(\mathbf{r})\|^2 \|\mathbf{a}_{T,\ell}(\mathbf{r})\|^2 \right\},$$

which enforces the use of *unit-norm* Tx-Rx Green vector functions  $\mathbf{a}_{T,\ell}/\|\mathbf{a}_{T,\ell}\|$  and  $\mathbf{a}_{R,\ell}/\|\mathbf{a}_{R,\ell}\|$ , as opposed to (3) (where unnormalized counterparts are employed) and (4) (where  $\mathbf{a}_{T,\ell}/\|\mathbf{a}_{T,\ell}\|^2$  and  $\mathbf{a}_{R,\ell}/\|\mathbf{a}_{R,\ell}\|^2$  are used instead). Such choice is in agreement with the intuitive rationale discussed in [20].

Secondly, it is interesting to compare the likelihood imaging in Eq. (5) with  $t_{\text{glr}}$  (adaptive case), which is rewritten as:

$$t_{\text{glr}}(\mathbf{r}) = \prod_{\ell=1}^L \|\mathbf{x}_\ell\|^2 / \left\| \mathbf{P}_{\mathbf{b}_\ell(\mathbf{r})}^\perp \mathbf{x}_\ell \right\|^2, \quad (12)$$

where the sole difference observed is the introduction of the numerator terms  $\|\mathbf{x}_\ell\|^2$ ,  $\ell = 1, \dots, L$ .

### III. INVARIANCE AND CFARNESS IN ADAPTIVE CASE

When referring to the adaptive case, it is desirable to build imaging functions which are insensitive to the unknown nuisance parameters  $\sigma_\ell^2$ ,  $\ell = 1, \dots, L$ , when no scatterer is present in the scene. To this end, we resort to the *principle of invariance* [18] applied to the hypothesis testing

<sup>3</sup>Indeed, it can be shown that all the three tests are statistically equivalent to one based on  $t_{\text{na}}$ .

<sup>4</sup>It is worth noticing that other well-founded decision statistics could be considered as well for the present composite hypothesis testing. These include the Durbin and Terrell (Gradient) statistics, as recently employed in [19]. However, it can be readily shown (the proof is left to the reader for brevity) that in this peculiar case they are both *statistically equivalent* to Rao test.

problem in (6), representing an elegant way for obtaining decision statistics (resp. tests) which ensure invariance (resp. a CFAR). To this end, hereinafter we will search for data functions sharing invariance w.r.t. those parameters (namely, the nuisance  $\sigma_\ell^2$ ,  $\ell = 1, \dots, L$ ) which are irrelevant for the decision problem considered. The preliminary step consists in finding transformations that properly cluster data without altering: (i) the structure of the hypothesis testing problem, i.e.  $\mathcal{H}_0 : |\tau_\ell| = 0$ ,  $\mathcal{H}_1 : \exists |\tau_\ell| > 0$  ( $\ell = 1, \dots, L$ ); (ii) the Gaussian assumption for the measured MDMs under each hypothesis; (iii) the scaled-identity structure of the noise covariance ( $\sigma_\ell^2 \mathbf{I}_N$ ) and the useful signal subspace. Of course, the group invariance requirement leads to a *lossy* data reduction, with the least compression embodied by the *Maximal Invariant Statistic* (MIS), organizing the original data into equivalence classes. Hence, every invariant statistic can be expressed in terms of the MIS [18]. For this reason, before proceeding, we first individuate a suitable group fulfilling the above requirements.

To this end, we take the (vectorized) single-source model in Eq. (2) and rewrite it in the so-called *canonical form*<sup>5</sup>:

$$\bar{\mathbf{x}}_\ell = \mathbf{e}_1 \bar{\tau}_\ell + \bar{\mathbf{w}}_\ell, \quad \ell = 1, \dots, L, \quad (13)$$

where  $\mathbf{e}_1 \triangleq \begin{bmatrix} 1 & \mathbf{0}_{N-1}^T \end{bmatrix}^T$ ,  $\bar{\tau}_\ell \in \mathbb{C}$  and  $\bar{\mathbf{w}}_\ell \sim \mathcal{CN}_N(\mathbf{0}_N, \sigma_\ell^2 \mathbf{I}_N)$ . The group of transformations leaving the hypothesis testing problem in (6) *unaltered* is represented by  $\mathbf{G} \triangleq \mathbf{G}_1 \times \dots \times \mathbf{G}_L$ , where  $\mathbf{G}_\ell$  is defined as follows:

$$\mathbf{G}_\ell \triangleq \{g_\ell : \bar{\mathbf{x}}_\ell \rightarrow \gamma_\ell \mathbf{V}_\ell \bar{\mathbf{x}}_\ell, \quad \gamma_\ell \in \mathbb{R}^+, \quad (14)$$

$$\mathbf{V}_\ell \triangleq \begin{bmatrix} e^{j\phi_\ell} & \mathbf{0}_{N-1}^T \\ \mathbf{0}_{N-1} & \mathbf{V}_{1,\ell} \end{bmatrix}, \quad \phi_\ell \in (0, 2\pi), \quad \mathbf{V}_{1,\ell} \in \mathcal{U}(N-1)\}$$

After defining the partitioning  $\bar{\mathbf{x}}_\ell = [\bar{x}_{a,\ell} \quad \bar{x}_{b,\ell}^T]^T$ , where  $\bar{x}_{a,\ell} \in \mathbb{C}$  and  $\bar{x}_{b,\ell} \in \mathbb{C}^{N-1}$ , respectively, we are able to state the proposition providing the MIS for the problem at hand.

**Proposition 1.** *The MIS for the hypothesis testing in Eq. (6) under the group  $\mathbf{G}$  is the  $L$ -dimensional vector:*

$$\mathbf{t} \triangleq [t_1 \quad \dots \quad t_L]^T, \quad t_\ell \triangleq |\bar{x}_{a,\ell}|^2 / \|\bar{x}_{b,\ell}\|^2. \quad (15)$$

*Proof:* The proof is readily obtained by extending the known result developed in the literature (see, e.g. [18]) for the simpler case  $L = 1$  and then exploiting the separability of the problem across the frequencies  $\omega_1, \dots, \omega_L$ . ■

For completeness, we remark that the MIS depends on the unknown parameters only through the corresponding induced maximal invariant [18], which for this specific case is  $\boldsymbol{\delta}^2 \triangleq [\delta_1^2 \quad \dots \quad \delta_L^2]$ , where  $\delta_\ell^2 \triangleq \frac{\|\mathbf{b}_\ell\|^2 |\tau_\ell|^2}{\sigma_\ell^2}$ , corresponding to the Signal-to-Noise Ratio (SNR) experienced on  $\omega_\ell$ .

Two important considerations are now in order. First, since the MIS in (15) is vector-valued *no Uniformly Most Powerful Invariant (UMPI) test exists* for the hypothesis testing in (6). Such negative result differs from that of the single-frequency ( $L = 1$ ) case, where  $t_1$  (i.e. a scalar-valued statistic) in Eq. (15) is also the UMPI decision statistic [17], [18].

<sup>5</sup>The canonical form representation is obtained by rotating each vector  $\mathbf{x}_\ell$  as  $\bar{\mathbf{x}}_\ell \triangleq \mathbf{U}_\ell^\dagger \mathbf{x}_\ell$ , where  $\mathbf{U}_\ell \triangleq \begin{bmatrix} \mathbf{b}_\ell \\ \|\mathbf{b}_\ell\| \end{bmatrix} \mathbf{U}_{c,\ell} \in \mathcal{U}(N)$ , that is, a unitary matrix whose first column is aligned toward the direction of  $\mathbf{b}_\ell$ .

Secondly, it can be shown (the proof is omitted for brevity) that the equality  $t_\ell = \Xi_\ell$  holds. Therefore, the MIS in Eq. (15) can be rewritten as  $\mathbf{t} = [\Xi_1 \ \cdots \ \Xi_L]^T \triangleq \Xi$ . Then, from direct comparison of MIS with statistics in Eq. (9) and, exploiting the theory in [18], it is readily deduced that the tests built on the aforementioned statistics, being functions of the original data  $\mathbf{x}_{1:L}$  solely through the MIS  $\Xi$ , are *invariant* and therefore they all *ensure* a CFAR w.r.t. the noise levels on the probed frequencies  $\sigma_\ell^2$ ,  $\ell = 1, \dots, L$ .

Additionally, following the first consideration, since no UMPI test exists, nothing can be said in advance on the relative performance of the aforementioned tests. For this reason, it is useful analyzing the structural properties of the (clairvoyant) MPI statistic<sup>6</sup>:

$$t_{\text{mpi}} \triangleq \frac{f_1(\Xi; \delta)}{f_0(\Xi; \delta = \mathbf{0}_L)} = \prod_{\ell=1}^L \frac{f_1(\Xi_\ell; \delta_\ell)}{f_0(\Xi_\ell; \delta_\ell = 0)}. \quad (16)$$

Clearly, since the corresponding MPI test depends on  $\delta^2$ , it *cannot* be implemented. However, since  $\Xi_\ell | \mathcal{H}_1 \sim \mathcal{CF}_{1, N-1}(\delta_\ell)$  and  $\Xi_\ell | \mathcal{H}_0 \sim \mathcal{CF}_{1, N}$  (these results are given, for example, in [21]) each ratio  $f_1(\Xi_\ell; \delta_\ell) / f_0(\Xi_\ell; \delta_\ell = 0)$ ,  $\ell = 1, \dots, L$ , is monotone with  $\Xi_\ell$  (since the complex non-central F-distribution is a totally-positive kernel of order 2, see [22]). Thus, it immediately follows that for each<sup>7</sup>  $\delta_1 \geq \delta_2$  the MPI detector is an *increasing function of the vector*  $\Xi$ .

Such key result allows to claim that *the space of monotone functions of*  $\Xi$  *forms a complete class* of decision statistics [23]. It thus follows that the GLR, Rao and Wald statistics in the multi-frequency case are all “meaningful” candidates, as they belong to the aforementioned class (cf. Eq. (9)). Remarkably, such consideration also applies to any other statistic built as an increasing function of  $\Xi$  (such as the geometric or harmonic means of the elements of  $\Xi$ ), which also represents a good candidate for a “stable” C-TR imaging.

#### IV. ADAPTIVE STATISTICS AS IMAGING PROCEDURES

This section first provides a statistical characterization of  $\Xi$  in the presence of a mismatch of the  $\mathbf{b}_\ell$ 's. This preliminary result will be useful to obtain the theoretical performance of the proposed statistics in the *realistic* case of multiple ( $M > 1$ ) scatterers (possibly with mutual interaction effect, i.e. a FL model). To this end, we assume a generic signal form  $\mathbf{x}_\ell \sim \mathcal{N}_C(\xi_\ell, \sigma_\ell^2 \mathbf{I}_N)$ ,  $\ell = 1, \dots, L$ . In this case, it holds  $(\mathbf{x}_\ell^\dagger \mathbf{P}_{\mathbf{b}_\ell} \mathbf{x}_\ell / \sigma_\ell^2) \sim \mathcal{C}\chi_1(\delta_{N,\ell})$  and  $(\mathbf{x}_\ell^\dagger \mathbf{P}_{\mathbf{b}_\ell}^\perp \mathbf{x}_\ell / \sigma_\ell^2) \sim \mathcal{C}\chi_{N-1}(\delta_{D,\ell})$ , where  $\delta_{N,\ell}^2 \triangleq (\xi_\ell^\dagger \mathbf{P}_{\mathbf{b}_\ell} \xi_\ell) / \sigma_\ell^2$  and  $\delta_{D,\ell}^2 \triangleq (\xi_\ell^\dagger \mathbf{P}_{\mathbf{b}_\ell}^\perp \xi_\ell) / \sigma_\ell^2$ , respectively. Consequently, in the mismatched case, it readily follows that  $\Xi_\ell \sim \mathcal{CF}_{1, N-1}(\delta_{N,\ell}, \delta_{D,\ell})$ .

Based on the above result, we now characterize statistically the obtained imaging functions for  $M > 1$  scatterers in the scene. Indeed, by vectorizing the model in Eq. (1), we get (using the short-hand notation  $\mathbf{M}_\ell$  for  $\mathbf{M}_\ell(\mathbf{r}_{1:M}, \boldsymbol{\tau}_\ell)$ ):

$$\mathbf{x}_\ell = [\mathbf{A}_{T,\ell}(\mathbf{r}_{1:M}) \otimes \mathbf{A}_{R,\ell}(\mathbf{r}_{1:M})] \text{vec}(\mathbf{M}_\ell) + \mathbf{w}_\ell. \quad (17)$$

<sup>6</sup>The MPI statistic is the likelihood-ratio after reduction by invariance (i.e. based on  $\Xi$ ).

<sup>7</sup>The notation  $\delta_1 \geq \delta_2$  means that each element of  $\delta_1$  is greater or equal than the corresponding element of  $\delta_2$ , and at least one element of  $\delta_1$  is strictly greater than the corresponding element of  $\delta_2$ .

By letting  $\xi_\ell = [\mathbf{A}_{T,\ell}(\mathbf{r}_{1:M}) \otimes \mathbf{A}_{R,\ell}(\mathbf{r}_{1:M})] \text{vec}(\mathbf{M}_\ell)$ , the mismatched analysis of Sec. III allows to conclude that the relevant information is *summarized* through  $\delta_{N,\ell}$  and  $\delta_{D,\ell}$ . Also, it can be shown that for the model in Eq. (17),  $\delta_{N,\ell}^2$  assumes the expression (when varying the *probed* location  $\mathbf{r}$ ):

$$\delta_{N,\ell}^2(\mathbf{r}) = \sigma_\ell^{-2} \text{vec}(\mathbf{M}_\ell)^\dagger [\mathbf{A}_{T,\ell}(\mathbf{r}_{1:M}) \otimes \mathbf{A}_{R,\ell}(\mathbf{r}_{1:M})]^\dagger \mathbf{P}_{\mathbf{b}_\ell(\mathbf{r})} \times [\mathbf{A}_{T,\ell}(\mathbf{r}_{1:M}) \otimes \mathbf{A}_{R,\ell}(\mathbf{r}_{1:M})] \text{vec}(\mathbf{M}_\ell), \quad (18)$$

whereas  $\delta_{D,\ell}^2(\mathbf{r})$  is obtained from (18) when replacing  $\mathbf{P}_{\mathbf{b}_\ell(\mathbf{r})}$  with  $\mathbf{P}_{\mathbf{b}_\ell(\mathbf{r})}^\perp$ . After tedious manipulations, these quantities can be rewritten in the more intuitive form:

$$\delta_{N,\ell}^2(\mathbf{r}) = \left\| \mathbf{h}_{R,\ell}^\dagger(\mathbf{r}) \mathbf{M}_\ell \mathbf{h}_{T,\ell}^*(\mathbf{r}) \right\|^2 / \sigma_\ell^2; \quad (19)$$

$$\delta_{D,\ell}^2(\mathbf{r}) = \left\{ \left\| \mathbf{A}_{R,\ell}(\mathbf{r}_{1:M}) \mathbf{M}_\ell \mathbf{A}_{T,\ell}^T(\mathbf{r}_{1:M}) \right\|_F^2 / \sigma_\ell^2 \right\} - \delta_{N,\ell}^2(\mathbf{r});$$

where we have defined the vector of normalized point-spread functions of the Tx (resp. Rx) array as  $\mathbf{h}_{T,\ell}(\mathbf{r}) \triangleq \{\mathbf{A}_{T,\ell}^\dagger(\mathbf{r}_{1:M}) \mathbf{a}_{T,\ell}(\mathbf{r})\} / \|\mathbf{a}_{T,\ell}(\mathbf{r})\|^2$  (resp.  $\mathbf{h}_{R,\ell}(\mathbf{r}) \triangleq \{\mathbf{A}_{R,\ell}^\dagger(\mathbf{r}_{1:M}) \mathbf{a}_{R,\ell}(\mathbf{r})\} / \|\mathbf{a}_{R,\ell}(\mathbf{r})\|^2$ ). Consequently, it readily follows that  $\Xi_\ell(\mathbf{r}) \sim \mathcal{CF}_{1, N-1}(\delta_{N,\ell}(\mathbf{r}), \delta_{D,\ell}(\mathbf{r}))$ ,  $\ell = 1, \dots, L$ , and the exact pdf of the random vector  $\Xi(\mathbf{r})$  can be expressed as  $\prod_{\ell=1}^L f_1(\Xi_\ell; \delta_{N,\ell}(\mathbf{r}), \delta_{D,\ell}(\mathbf{r}))$ . Then, the pdfs of GLR, Rao and Wald imaging functions can be obtained by *transformation* of vector  $\Xi(\mathbf{r})$ , see Eq. (9). The preceding analysis is also employed to provide a theoretical characterization of the imaging functions in Eqs. (3-4-5-11), as shown hereinafter.

*MF imaging:* The function  $\text{I}_{\text{tr}}(\mathbf{r}, \ell)$  in (3) can be rewritten by exploiting  $\mathbf{a}_{R,\ell}^\dagger(\mathbf{r}) \mathbf{X}_\ell \mathbf{a}_{T,\ell}^*(\mathbf{r}) = \mathbf{b}_\ell^\dagger(\mathbf{r}) \mathbf{x}_\ell$  (achieved with the use of  $\text{vec}(\cdot)$  and Kronecker product properties), thus leading to  $\text{I}_{\text{tr}}(\mathbf{r}, \ell) / (\|\mathbf{b}_\ell(\mathbf{r})\|^2 \sigma_\ell^2) \sim \mathcal{C}\chi_1(\delta_{N,\ell}(\mathbf{r}))$ , which in turn provides

$$\text{I}_{\text{tr}}(\mathbf{r}, \ell) \sim \mathcal{C}\chi_1 \left( \delta_{N,\ell}(\mathbf{r}), \sigma_\ell^2 \|\mathbf{b}_\ell(\mathbf{r})\|^2 \right). \quad (20)$$

*ML imaging:* By similar reasoning as MF imaging,  $\text{I}_{\text{ml}}(\mathbf{r}, \ell)$  in (4) is distributed as (recall that  $\|\mathbf{b}_\ell(\mathbf{r})\|^2 = \|\mathbf{a}_{T,\ell}(\mathbf{r})\|^2 \|\mathbf{a}_{R,\ell}(\mathbf{r})\|^2$ ):

$$\text{I}_{\text{ml}}(\mathbf{r}, \ell) = \mathcal{C}\chi_1 \left( \delta_{N,\ell}(\mathbf{r}), \sigma_\ell^2 / \|\mathbf{b}_\ell(\mathbf{r})\|^2 \right). \quad (21)$$

*Likelihood imaging:* The imaging function  $\text{I}_{\text{li}}(\mathbf{r})$  in Eq. (5) can be rewritten as  $\text{I}_{\text{li}}(\mathbf{r}) = (\prod_{\ell=1}^L \sigma_\ell^2 f_\ell)^{-1}$ , where  $f_\ell \sim \mathcal{C}\chi_{N-1}(\delta_{D,\ell}(\mathbf{r}))$ ,  $\ell = 1, \dots, L$ .

*Non-adaptive imaging:* It can be easily shown that  $t_{\text{na}}(\mathbf{r})$  in (11) is distributed as  $t_{\text{na}}(\mathbf{r}) \sim \mathcal{C}\chi_1(\delta_{N,\ell}(\mathbf{r}))$ . We recall that such function requires the knowledge of  $\sigma_\ell^2$ ,  $\ell = 1, \dots, L$ , which may be not known in an adaptive scenario.

#### V. SIMULATION ANALYSIS

In this section we focus on 2-D localization in a homogeneous background, where the relevant (scalar) background Green function at  $\omega_\ell$  is<sup>8</sup>  $\mathcal{G}_\ell(\mathbf{x}', \mathbf{x}) = H_0^{(1)}(\kappa_\ell \|\mathbf{x}' - \mathbf{x}\|)$ , [9]. Here  $H_n^{(1)}(\cdot)$  and  $\kappa_\ell = 2\pi/\lambda_\ell$  denote the  $n$ th order *Hankel* function of the 1st kind and the wavenumber ( $\lambda_\ell$  is the wavelength corresponding to  $\omega_\ell$ ), respectively.

<sup>8</sup>We discard the irrelevant constant term  $j/4$ .

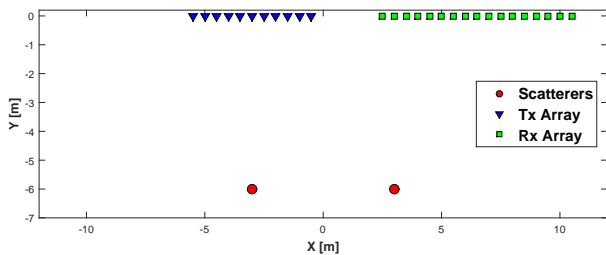


Figure 1. Geometry for the considered imaging problem in 2-D space.

In what follows, we consider a non-co-located setup with half-meter spaced Tx/Rx arrays displaced as shown in Fig. 1 ( $N_T = 11$  and  $N_R = 17$ , in blue “ $\nabla$ ” and green “ $\square$ ” markers, respectively). For this scenario, we consider  $L = 3$  frequencies for active probing, with considered frequencies equal  $(f_1, f_2, f_3) = (300, 600, 900)$  MHz (recall that  $f_\ell = \omega_\ell/2\pi$ ), corresponding to  $(\lambda_1, \lambda_2, \lambda_3) = (1, 0.5, 0.333)$  m. For this example, the noise variance levels  $\sigma_\ell^2$  pertaining to the considered frequencies are set to  $(\sigma_1^2, \sigma_2^2, \sigma_3^2) = (-15, -5 - 15)$  dB.

For simplicity, we consider  $M = 2$  targets in the considered area, located at  $\mathbf{x}_1 = [-1 \ -6]^T$  m and  $\mathbf{x}_2 = [+1 \ -6]^T$  m (reported as red “o” markers in Fig. 1) and having scattering coefficients  $\boldsymbol{\tau}_\ell = [3 \ 4]^T$ . For the aforementioned scenario, we report the averaged (over 100 independent runs) spectrum of the imaging functions (i)  $\log[t_{\text{glr}}(\mathbf{r})]$ , (ii)  $t_{\text{rao}}(\mathbf{r})$ , (iii)  $t_{\text{wald}}(\mathbf{r})$  and (iv)  $\log[I_{\text{li}}(\mathbf{r})]$  being proposed/investigated in this letter. We remark that, aiming at a fair comparison, GLR- and likelihood-imaging have been reported in their log-versions, so as to compare all the imaging functions in terms of sums of contributions over the considered frequencies.

In Fig. 2 we show the results corresponding to BA scattering model, whereas the corresponding results for FL model are reported in Fig. 3. From inspection of both the figures, it is apparent that the proposed imaging functions (being based on statistical testing and designed to enjoy weak-sensitivity to  $\sigma_\ell^2$ s) offer an improved contrast in resolving the two scatterers considered in comparison to likelihood-imaging. Those imaging functions are also observed to exhibit a more stable behaviour with a varying level of noise power. Also, they are observed to perform all equally well, as apparent from Figs. 2 and 3, respectively. Indeed, their relative performance varies from case to case and reflects non-optimality of all the considered testing procedures for finite samples, see [17].

Finally, useful considerations can be drawn on the relative performance in both the cases of BA (Fig. 2) and FL (Fig. 3) scattering models. Indeed, in the case of FL scattering, a higher distortion is generally observed w.r.t. BA case. This is mainly due to the non-linearity of the scattering model, which is not accounted by all the considered procedures, being based on a single-target model assumption (and thus not reflecting mutual interaction effects).

## VI. CONCLUSIONS

In this letter imaging functions for wideband C-TR have been devised based on GLR, Rao and Wald statistics under the

single-source model. Both non-adaptive and adaptive (where a supporting CFAR analysis through invariance principle has been provided) have been analyzed. The proposed imaging functions have been also compared with other imaging functions proposed in the literature. For all these functions a theoretical characterization for the multiple-scatterers case (possibly with mutual interaction) has been derived and shown to depend only on the non-centrality parameter functions  $\delta_{N,\ell}(\mathbf{r})$  and  $\delta_{D,\ell}(\mathbf{r})$  (Eq. (19)).

## REFERENCES

- [1] M. Fink, “Time-reversal mirrors,” *J. Phys. D: Appl. Phys.*, vol. 26, no. 9, p. 1333, 1993.
- [2] D. Cassereau and M. Fink, “Time-reversal of ultrasonic fields. III. theory of the closed time-reversal cavity,” *IEEE Trans. Ultrason., Ferroelectr., Freq. Control*, vol. 39, no. 5, pp. 579–592, Sep. 1992.
- [3] J. W. Odendaal, E. Barnard, and C. W. I. Pistorius, “Two-dimensional superresolution radar imaging using the MUSIC algorithm,” *IEEE Trans. Antennas Propag.*, vol. 42, no. 10, pp. 1386–1391, Oct. 1994.
- [4] G. Micolau, M. Saillard, and P. Borderies, “DORT method as applied to ultrawideband signals for detection of buried objects,” *IEEE Trans. Geosci. Remote Sens.*, vol. 41, no. 8, pp. 1813–1820, Aug. 2003.
- [5] L. Li, W. Zhang, and F. Li, “A novel autofocusing approach for real-time through-wall imaging under unknown wall characteristics,” *IEEE Trans. Geosci. Remote Sens.*, vol. 48, no. 1, pp. 423–431, Jan. 2010.
- [6] M. D. Hossain, A. S. Mohan, and M. J. Abedin, “Beamspace time-reversal microwave imaging for breast cancer detection,” *IEEE Antennas Wireless Propag. Lett.*, vol. 12, pp. 241–244, 2013.
- [7] G. Shi and A. Nehorai, “Cramér-Rao bound analysis on multiple scattering in multistatic point-scatterer estimation,” *IEEE Trans. Signal Process.*, vol. 55, no. 6, pp. 2840–2850, Jun. 2007.
- [8] D. Ciuonzo, G. Romano, and R. Solimene, “Performance analysis of time-reversal MUSIC,” *IEEE Trans. Signal Process.*, vol. 63, no. 10, pp. 2650–2662, 2015.
- [9] A. J. Devaney, “Time reversal imaging of obscured targets from multistatic data,” *IEEE Trans. Antennas Propag.*, vol. 53, no. 5, pp. 1600–1610, May 2005.
- [10] C. Prada, S. Manneville, D. Spoliansky, and M. Fink, “Decomposition of the time reversal operator: Detection and selective focusing on two scatterers,” *The Journal of the Acoustical Society of America*, vol. 99, no. 4, pp. 2067–2076, 1996.
- [11] D. Ciuonzo and P. Salvo Rossi, “Noncolocated time-reversal MUSIC: High-SNR distribution of null spectrum,” *IEEE Signal. Proc. Lett.*, vol. 24, no. 4, pp. 397–401, 2017.
- [12] P. Stoica and Y. Selen, “Model-order selection: a review of information criterion rules,” *IEEE Signal. Proc. Mag.*, vol. 21, no. 4, pp. 36–47, 2004.
- [13] L. Borcea, G. Papanicolaou, and C. Tsogka, “Theory and applications of time reversal and interferometric imaging,” *Inverse Problems*, vol. 19, no. 6, pp. 139–164, 2003.
- [14] G. Shi and A. Nehorai, “Maximum likelihood estimation of point scatterers for computational time-reversal imaging,” *Communications in Information & Systems*, vol. 5, no. 2, pp. 227–256, 2005.
- [15] —, “A relationship between time-reversal imaging and maximum-likelihood scattering estimation,” *IEEE Trans. Signal Process.*, vol. 55, no. 9, pp. 4707–4711, Sep. 2007.
- [16] M. A. Richards, J. A. Scheer, and W. A. Holm, *Principles of Modern Radar Volume I-Basic Principles*. Scitech Publishing, 2010.
- [17] S. M. Kay, *Fundamentals of Statistical Signal Processing, Volume 2: Detection Theory*. Prentice Hall PTR, Jan. 1998.
- [18] E. L. Lehmann and J. P. Romano, *Testing statistical hypotheses*. Springer Science & Business Media, 2006.
- [19] D. Ciuonzo, A. De Maio, and D. Orlando, “A unifying framework for adaptive radar detection in homogeneous plus structured interference - Part II: detectors design,” *IEEE Trans. Signal Process.*, vol. 64, no. 11, pp. 2907–2919, Jun. 2016.
- [20] L. Borcea, G. Papanicolaou, C. Tsogka, and J. Berryman, “Imaging and time reversal in random media,” *Inverse Problems*, vol. 18, no. 5, p. 1247, 2002.
- [21] J. Liu, W. Liu, B. Chen, H. Liu, and H. Li, “Detection probability of a CFAR matched filter with signal steering vector errors,” *IEEE Signal Process. Lett.*, vol. 22, no. 12, pp. 2474–2478, 2015.
- [22] S. Karlin, *Total positivity*. Stanford University Press, 1968, vol. 1.

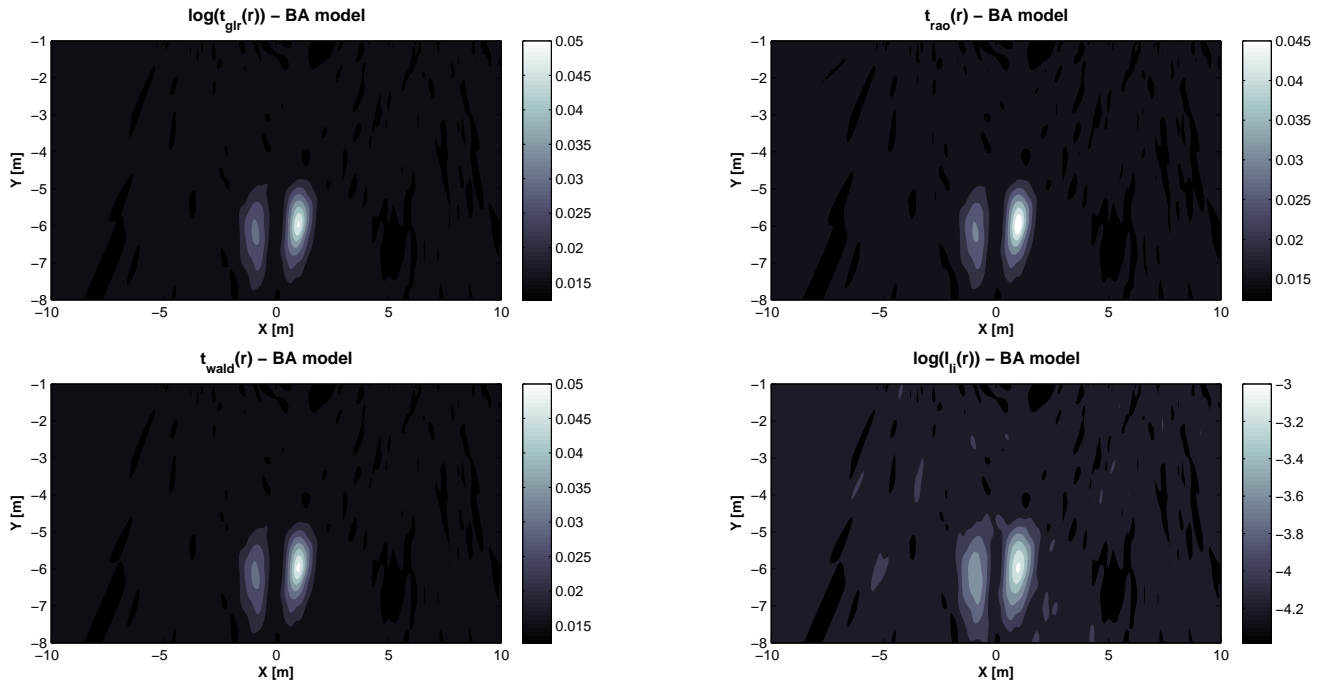


Figure 2. Comparison of considered imaging functions; BA scattering model. Scatterers are located at  $\mathbf{x}_1 = [-1 \quad -6]^T$  m and  $\mathbf{x}_2 = [+1 \quad -6]^T$  m.

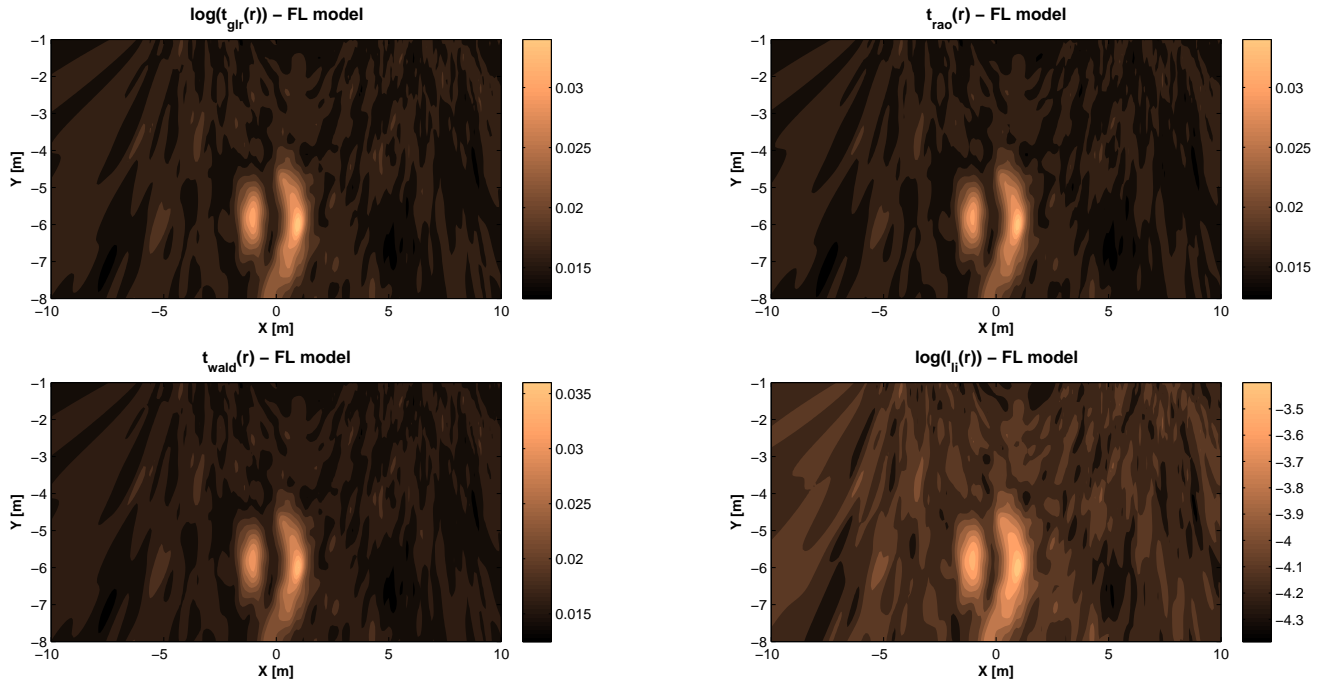


Figure 3. Comparison of considered imaging functions; FL scattering model. Scatterers are located at  $\mathbf{x}_1 = [-1 \quad -6]^T$  m and  $\mathbf{x}_2 = [+1 \quad -6]^T$  m.

- [23] L. D. Brown, A. Cohen, and W. E. Strawderman, "A complete class theorem for strict monotone likelihood ratio with applications," *The Annals of Statistics*, vol. 4, no. 4, pp. 712–722, 1976.